

Viewing angle of holographic image reconstructed from digital hologram with enhanced numerical aperture

Byung Gyu Chae

*Biomedical Imaging Group, Electronics and Telecommunications Research Institute,
218 Gajeong-ro, Yuseong-gu, Daejeon, 34129, Republic of Korea*

Abstract

The digital hologram with enhanced numerical aperture (NA) forms the replica fringe pattern in the Fresnel diffraction regime, which reconstructs the respective multiple images. The viewing angle of reconstructed multiple images is interpreted from the quantum mechanical uncertainty relation between the momentum of photon field and its spatial resolution. The multiple images have the same viewing angle represented as the NA of whole aperture of hologram other than subaperture of replica fringe patterns. Optical experiment shows the consistent result with quantum mechanical interpretation of viewing angle of holographic images. We discuss the method for enlarging viewing angle of holographic image without sacrificing image size by using this property.

I. INTRODUCTION

The holographic display is an optical imaging system that reconstructs the real or imaginary image in a free space from the digital hologram [1–4]. The spatial resolution of the holographic image in digital holography follows the Rayleigh criterion related to the numerical aperture [5–7]. We suggested that the angular field view of reconstructed image in holography display is fundamentally determined by the numerical aperture (NA) of digital hologram [8]:

$$\Omega = 2 \sin^{-1} \left(\frac{N\Delta x}{2z} \right). \quad (1)$$

The viewing angle Ω depends on only the geometrical structures of lateral size, $L = N\Delta x$ and distance z . The angle value is irrespective of the diffraction ability from the pixel size Δx or a wavelength λ of incident wave. This is not straightforward in some ways because the diffraction scope of the pixel seems to define the viewing zone. However, we observed that the variation of viewing angle well obeys the relation of Eq. (1).

The extension of viewing angle is a crucial task for realizing the holographic display. Principally, the hologram numerical aperture can be enhanced in the digital hologram synthesized at a closer distance. When the digital hologram is made at a distance lower than a critical distance, $z_c = N\Delta x^2/\lambda$, the viewing angle would be higher than the diffraction angle from the pixel pitch. We defined this type of hologram as the enhanced-NA hologram [9]. On the other hand, the statement is not simple because the hologram fringe undergoes the aliasing effects in this circumstance when being sampled. The sampling condition has clearly understood in the Nyquist sampling theorem with respect to both planes or by the Wigner domain description [10–13]. The aliased fringe is repeated over the entire hologram according to the extent of undersampling, which also generates replications of the reconstructed image.

The resolution of the reconstructed image is theoretically interpreted by the window function covering the hologram aperture. The whole area of the hologram is adopted as the aperture range without sufficient foundation, where it is not certain why the whole area of the hologram aperture contributes to the formation of respective images.

The purpose of this study is to provide a valid foundation to describe the viewing angle of holographic images in terms of the NA of the whole area in the hologram. Firstly,

we investigate the internal structure of the point spread function (PSF) revealed in the sampling environment through mathematical and numerical approaches. From this, we find out the self-similarity of modulating curves in the sampled kernel function. Secondly, on the basis of quantum mechanical framework, we analyze the viewing angle of holographic image reconstructed from the enhanced-NA hologram. Finally, we carry out the optical experiments for observing the viewing angle variation dependent on the hologram numerical aperture, and discuss the possibility for realizing the holographic display with a wide viewing angle by using this interpretation.

II. FRACTAL STRUCTURE OF MODULATING CURVES IN SAMPLED POINT SPREAD FUNCTION

The Fresnel diffraction field is well described by the convolutional kernel function $h(x, y)$ of the PSF [1],

$$h(x, y) = \frac{e^{ikz}}{i\lambda z} \exp\left[i\frac{\pi}{\lambda z}(x^2 + y^2)\right] \quad (2)$$

where k is a wavenumber expressed as $2\pi/\lambda$, and z is a distance between object plane and hologram plane. The PSF reveals the interesting mathematical properties because of a quadratic phase term when being sampled [14]. The Fourier transform **FT** of sampled PSF in one-dimensional description is written by

$$\mathbf{FT} \left(\sum_n h(n\Delta x)\delta(x - n\Delta x) \right) = \frac{1}{\Delta x} \sum_q H \left(f - \frac{q}{\Delta x} \right), \quad (3)$$

where Δx is the sampling period. $H(f)$ is also a quadratic phase function of spatial frequency $f = x/\lambda z$, which is called a optical transfer function. The term in the summation of Eq. (3) can be expressed as the modulation of H function, $c_{q/\Delta x}H(f) \exp(i2\pi\lambda z f/\Delta x)$ where $c_{q/\Delta x} = \exp(-i\pi\lambda z q^2/\Delta x^2)$, and thus, we can get following equality,

$$\sum_n h(n\Delta x)\delta(x - n\Delta x) = \frac{1}{\Delta x} \sum_q c_{q/\Delta x} h \left(x + \frac{\lambda z q}{\Delta x} \right). \quad (4)$$

The sampling of PSF induces the replication of the weighted original function with a period of $\lambda z/\Delta x$, which does not make a meaningless aliased fringe when being sampled. This implies that the PSF undersampled by s multiples of Δx forms the replica functions at

a reduced period of $\lambda z/s\Delta x$. We can also extract the minimum distance z_c for the function with N samples without inducing replication as follows, $z_c = N\Delta x^2/\lambda$.

Figure 1 displays a quadratic sinusoid of sampled kernel function. The magnitude of curves seems to be very irregular unlike the analog signal, but the curves include their internal structure. If one divide the function of Eq. (4) into two parts, sampled by even numbers n_e and odd numbers n_o , i.e., $\sum_{n_e} h(n_e\Delta x)\delta(x - n_e\Delta x) + \sum_{n_o} h(n_o\Delta x)\delta(x - n_o\Delta x)$, each term also consists of replica functions with an interval $\lambda z/(2\Delta x)$:

$$\left[c_0 h(x) + c_1 h\left(x + \frac{\lambda z}{2\Delta x}\right) \right]_{\text{even}} + \left[c_0 h(x) + c_1 h\left(x + \frac{\lambda z}{2\Delta x}\right) \right]_{\text{odd}}. \quad (5)$$

Similarly, each term of Eq. (5) can be resampled into two parts, and when the function is successively sampled by an s -fold sampling period, the replica patterns divided by the s -fold are generated, as depicted in Figs. 1(a) and 1(b).

Furthermore, the sampled kernel function has the modulating curves of original function according to geometrical placement. Let us incorporate two terms of Eq. (5). The incorporation of two terms results in a twofold increase in sampling rate. The primary Fresnelet centered on the axis simply becomes original form. Meanwhile, the secondary Fresnelet should be made using the specifications $(z/2, \Delta x)$ in a view of its placement [9], and thus, they would be modified in the form using a sampling rate Δx^{-1} :

$$\exp\left[\frac{i\pi}{\lambda z/2}\left(x + \frac{\lambda z/2}{\Delta x}\right)^2\right]. \quad (6)$$

The secondary Fresnelet has a phase coefficient of $(\lambda z/2)^{-1}$, and appears as the modulation of complex exponential function, which is clearly confirmed in the boundary curve of Figs. 1(a) and 1(b). Since the width δX of core shell of primary Fresnelet is given by

$$-\sqrt{\lambda z} \leq \delta X \leq \sqrt{\lambda z}, \quad (7)$$

the secondary Fresnelet has the core shell width of $(1/\sqrt{2})\delta X$, which is also confirmed in two-dimensional Fresnel zones of Fig. 2. Likewise, the value in the subsidiary Fresnelets digitized by s -fold sampling period would be

$$\left(\frac{1}{\sqrt{s}}\right)\delta X. \quad (8)$$

Above characteristics induces a self-similar structure of modulating curves of PSF. The similar subsidiary curves are recursively created in arbitrary sampled PSF, depending on two internal variables ($z, \Delta x$) of distance and sampling period. Figure 2 shows the fractal structure of two-dimensional Fresnelet for angle-valued kernel function. The similar zones in a small scale are emerged when magnifying the pattern, where the number of smaller zones increases fourfold at half the scale parameter. This is a typical fractal characteristic with a Hausdorff fractal dimension of two [15]. However, we can observe that the structure in two-dimensional space is somewhat complicate. Since the description based on Eq. (5) relates to only the multiple of sampling period $2\Delta x$, other sampling periods as like $3\Delta x$ and $5\Delta x$ should be considered to analyze the similar patterns completely. The subsidiary zones created by sampling period of prime number pixel $3\Delta x$ appear in Fig. 2, which could also create their self-similar zones, where a Hausdorff dimension is still two. We find that in the Fresnelet fractal, the fractal structures with respect to various sampling periods are mixed.

Let us consider the synthesis of enhanced-NA hologram. In digital hologram synthesized at a half of z_c , the modulating curve of Eq. (6) becomes in the form of Fresnel zones. This fractal property of modulating curve makes adaptively the well-behaved replications of Fresnel zones in accordance with a decrease of distance.

III. VIEWING ANGLE ANALYSIS OF RECONSTRUCTED IMAGE FROM ENHANCED-NA HOLOGRAM

We investigate the property of viewing angle of the holographic image reconstructed from the enhanced-NA hologram. The Fresnel diffraction field $g(x, y)$ is represented by the convolution of the optical kernel function with the object field $o(x, y)$,

$$g(x, y) = o(x, y) * h(x, y). \quad (9)$$

In an on-axis point object of delta function, the real or imaginary value of the kernel function $h(x, y)$ becomes a hologram in the form of a Fresnel zone [16], where as described in the previous section, the replica patterns of Fresnel zone can be generated at below the z_c -distance.

Let us unwrap the phase hologram of point object. As illustrated in Figs. 1(c) and 3(a), the unwrapped phase synthesized at a critical distance z_c reveals the single Fresnel lens

with smooth curvature. We know that the single Fresnel lens acts like Fourier lens to focus the incident wave to a point spot. In case of the enhanced-NA hologram synthesized at a distance lower than z_c , the multiple Fresnel lens are formed in Fig. 3(b). They can generate the multiple point images from the incident plane wave. It has been studied that the point images have an equally distributed intensity [17, 18].

The spatial resolution R of focused image is subject to the Rayleigh criterion described by hologram numerical aperture [5, 7]:

$$R = 0.61 \frac{\lambda}{\text{NA}}. \quad (10)$$

Numerical aperture is expressed as the geometric structure of aperture size, $L = N\Delta x$ and distance z , $\text{NA} = \sin \Omega_{\text{NA}} = N\Delta x/2z$. The total spatial extent L of digital hologram becomes the aperture window in a single Fresnel lens, whereas in case of s multiple lens in Fig. 4, it looks like that the aperture magnitude is the spatial size of the individual lens, written as the L/s . This would be natural phenomenon when the unit Fresnel lenses are isolated each other physically or when the low-pass filtering of the hologram fringe appears during the hologram synthesis by a convolutional method [8]. Here, the individual lens function are spread over whole area of the hologram, which are continuously connected in a view of photon field. In this situation, it is not certain whether or not only the part of digital hologram is used as aperture window.

For the further analysis of viewing angle of the image, it is required the quantum mechanical approach because the incident photon field goes through the whole area of digital hologram as one aperture. The quantized field acts as individual photons with momentum, $p = h/\lambda$, where h is the Planck constant. The spatial resolution of the image is written by

$$R \cong \frac{\lambda}{\text{NA}} = \frac{h}{p \sin(\Omega/2)}. \quad (11)$$

Putting the photon momentum in the lateral direction as $p_r = p \sin(\Omega/2)$, above equation indicates the Heisenberg uncertainty relation [19], $\Delta R \Delta p_r \geq h/2$. From this, as illustrated in Fig. 4, we find that the spatial resolution of the corresponding images to the replication Fresnel lens has the same value generated from the hologram numerical aperture with whole aperture window.

Considering a real object as a collection of points, the hologram is synthesized by the

summation of the Fresnel zones, where the off-axis point object placed at (a, b) in lateral coordinates is given by $h(x - a, y - b)$. Applying the rectangular function $\text{rec}(\frac{x}{L})$ of whole aperture window to the respective replication functions, we obtain the following convolution relation for the restored image of an arbitrary object:

$$\sum_q o\left(x' + \frac{\lambda z q}{\Delta x}\right) * \text{sinc}\left(\frac{\pi L x'}{\lambda z}\right). \quad (12)$$

The width of the first maximum peak of a sinc function defines an image resolution limit resolving the closest points. All reconstructed replica images have the same resolution limit and thus, appears with the same viewing angle Ω of a holographic image in Eq. (1).

IV. OPTICAL HOLOGRAM IMAGING FOR ENHANCED-NA HOLOGRAM

Figure 5 illustrates the configuration of the in-line holographic system used to synthesize the enhanced-NA hologram at a distance z_{en} lower than z_c . In order to avoid the aliased error in the process of hologram synthesis, the size of object should be confined to the diffraction region by the hologram pixel, and thus, it decreases with decreasing the synthesis distance. On the other hand, as studied in our previous work [9], although the sampling condition with respect to the object plane is well satisfied, the aliased error in the hologram plane occurs, which makes the replica fringe from the undersampling of digital hologram.

The synthesized digital holograms are shown in Fig. 6. Two letter objects separated from each other in the axial direction are vertically stacked on the coaxial x -axis. The latter object is placed at half the distance of z_c , 15.4 mm. Here, the distance z_c for the object with 256×256 pixels and a pixel pitch of $8 \mu\text{m}$ is 30.8 mm. The four aliased fringes in two-dimensional space are presumed to be formed from the undersampling of Fresnel factor. The Gerchberg-Saxton iterative algorithm is applied to extract the phase hologram [20]. The replica fringe is spatially created in Fig. 6(c). We note that the replica fringe of the former letter is placed at a shifted position vertically or horizontally. This phenomenon is natural because geometrically, the replica fringe is generated by different perspective view of two objects in comparison to central fringe. In the reconstruction process, the replica fringes will restore the corresponding images at their respective locations, which coincide with the high-order reconstructed images by the pixel pitch of the digital hologram.

Figure 7 shows the optically reconstructed images for the enhanced-NA digital holograms.

We used a phase spatial light modulator (Holoeye PLUTO) with 1920×1080 pixels and a pixel pitch of $8 \mu\text{m}$ along with a 473-nm blue laser as the source of incident plane wave. The z_c -distance for x -direction is calculated to be 259.8 mm. The restored image from the hologram made using the objects located at half the distance of z_c , 129.9 mm, is displayed in Fig. 7(a). Here, two letter objects are located at a distance of 20 mm. Several high-order images are captured within the lens aperture of the camera. The high-order images of the reconstructed image are placed at the positions specified in the synthesized hologram. We also observe that the first-order image of the former letter is placed at a horizontally shifted position owing to a different perspective view. Since the viewing direction of captured image is set to be zeroth-order image, the images adjacent to the central image show their perspective views. We can confirm that the perspective view of the central image is changed by moving the viewing direction to the adjacent image, in Fig. 7(b). The viewing angle is estimated to be 7.1° from the maximum perspective view of the reconstructed image, which is similar to the value 6.8° , calculated from the whole aperture of the hologram. This means that all images reconstructed optically from the hologram fringes have the same viewing angle with respect to the whole aperture of the digital hologram. That is, the corresponding aperture size is not limited to the area within the boundary of each fringe.

Figure 7(c) is the restored image for the objects located at quarter the distance of z_c , 64.9 mm. For convenience, two letter objects are separated by a distance of 10 mm. We can see up to the second-order restored image within the diffraction zone with respect to an object pixel pitch of $2 \mu\text{m}$. The former letter image is shifted twice in comparison to the first-order image, and the viewing angle of the second images is estimated to be 14.8° . The restored image from the holograms synthesized using the objects placed at a distance of 32.5 mm is displayed in Fig. 7(d). We can see up to the fourth-order images where the distance between two objects is 5 mm, and the estimated maximum viewing angle is appeared to be 28.1° . The perspective views of all orders of images are clearly confirmed by changing the viewing direction to the respective images. Figure 7(e) is a plot of the variations in the viewing angle of holographic image as a function of the synthesis distance, where the simulated curve is based on Eq. (1). It is noted that holographic image with a high viewing angle can be obtained at a shorter distance.

V. DISCUSSIONS FOR WIDE VIEWING-ANGLE HOLOGRAPHIC DISPLAY

The replicated fringes in the enhanced-NA hologram are continuous over the entire hologram in Eq. (4), but the aperture size seems to be confined in the region of each fringe. In a view of classical wave optics, the reconstructed images have an equally distributed intensity [17, 18], and seem to have the reduced viewing angle due to subaperture of each fringe. However, the result of optical experiment shows the increase of viewing angle in the enhanced-NA hologram, which is consistent with the analysis within the quantum mechanical description. As previously described, the incident photon field on the digital hologram experiences a whole area as one aperture. The replications of the Fresnel zones are seamlessly connected other than the physically isolated lens array. The self-similar property of kernel function appearing in the form of modulating curve makes it possible to form well-behaved replica fringes.

For realizing the wide viewing-angle holographic display, the increase of viewing angle should be feasible without sacrificing the image size, and furthermore, the interference of high-order images should be removable when we view the holographic image. In our previous work [8], we have shown that the digital Fresnel hologram synthesized using the extended object out of the diffraction region of hologram pixel has not aliased fringes, which is resulted from the property that the object light is straight forward in the Fresnel regime to suppress the replica fringes. Although the original object is well reconstructed in numerical simulation, its optical reconstruction strongly depends on the performance of spatial light modulation. Here, the concentration of hologram fringe makes it difficult to modulate the incident light. Several researches have been carried out to recover the concentration of hologram fringe. The additional factors such as the random-phase or virtual convergence light are used to diffuse the object light in the hologram synthesis [21–23]. In addition, present spatial light modulators are capable of modulating only the phase or amplitude hologram. The practical phase hologram is obtainable by means of the iterative optimization algorithms.

In this circumstance, the formation of replica fringes is inevitable during synthesizing enhanced-NA hologram. As described in Section 2, the replica fringe is generated from the sampling rate lower than the proper sampling rate. We know that this phenomenon arises from the sub-sampling by a multiple pixel pitch, as displayed in Figs. 1(a) and 1(b). If the

sub-sampling is performed by an irregular pixel pitch, there appears no replica fringe. If there is also an irregularly pixelated spatial light modulator which has nonuniformly distributed pixels of irregular pixel size, it would effectively hinder the formation of replica fringe. In this case, the digital hologram without replica fringes can be synthesized even using the extended object field of view, and thus, the wide-angle holographic display without sacrificing image size would be realized [24]. This approach can solve the narrow viewing-angle known as a crucial bottleneck in realizing the holographic display, but there still remain other problems to be solved, as like non-diffraction beam and twin image.

VI. CONCLUSIONS

The viewing angle of holographic image in the enhanced-NA digital hologram is well interpreted from the quantum mechanical uncertainty relation. The self-similarity of optical kernel function becomes an origin in adaptively forming the replications of hologram fringe pattern generating the respective multiple images. The viewing angle of replica images has the same value represented as the NA of whole aperture of hologram. Optical experiment shows the consistent result with the quantum mechanical analysis of viewing angle dependent on the hologram numerical aperture. This interpretation could give the method for enlarging the viewing angle of holographic image in holographic display by using a technology protecting the formation of replica fringe.

This work was partially supported by Institute for Information & Communications Technology Promotion (IITP) grant funded by the Korea government (MSIP) (2017-0-00049)

-
- [1] J. W. Goodman, *Introduction to Fourier Optics* (McGraw-Hill, 1996).
 - [2] T. Kozacki, M. Kujawińska, G. Finke, B. Hennelly, and N. Pandey, “Extended viewing angle holographic display system with tilted SLMs in a circular configuration,” *Appl. Opt.* 51(11), 1771-1780 (2012).
 - [3] J. Hahn, H. Kim, Y. Lim, G. Park, and B. Lee, “Wide viewing angle dynamic holographic stereogram with a curved array of spatial light modulators,” *Opt. Express* 16(16), 12372-12386 (2008).

- [4] M. Park, B. G. Chae, H. Kim, J. Hahn, H. Kim, C. H. Park, K. Moon, and J. Kim, "Digital holographic display system with large screen based on viewing window movement for 3D video service," *ETRI J.* 36(2), 232-241 (2014).
- [5] T. Latychevskaia and H.-W. Fink, "Inverted Gabor holography principle for tailoring arbitrary shaped three-dimensional beams," *Sci. Rep.* 6, 26312 (2016).
- [6] D. P. Kelly, B. M. Hennelly, N. Pandey, T. J. Naughton, and W. T. Rhodes, "Resolution limits in practical digital holographic systems," *Opt. Eng.* 48(9), 95801 (2009).
- [7] P. Picart and J. Leval, "General theoretical formulation of image formation in digital Fresnel holography," *J. Opt. Soc. Am. A* 25(7), 1744-1761 (2008).
- [8] B. G. Chae, "Analysis on angular field of view of holographic image dependent on hologram numerical aperture in holographic display," *Opt. Eng.* 59(3), 035103 (2020).
- [9] B. G. Chae, "Analysis on image recovery for on-axis digital Fresnel hologram with aliased fringe generated from self-similarity of point spread function," *Opt. Commun.* 466, 125609 (2020).
- [10] D. Mas, J. Garcia, C. Ferreira, L. M. Bernardo, and F. Marinho, "Fast algorithms for free-space diffraction patterns calculations," *Opt. Commun.* 164, 233-245 (1999).
- [11] A. Stern and B. Javidi, "Improved-resolution digital holography using the generalized sampling theorem for locally band-limited fields," *J. Opt. Soc. Am. A* 23(5), 1227-1235 (2006).
- [12] D. G. Voelz and M. C. Roggemann, "Digital simulation of scalar optical diffraction: revisiting chirp function sampling criteria and consequences," *Appl. Opt.* 48(32), 6132-6142 (2009).
- [13] J.-P. Liu, "Controlling the aliasing by zero-padding in the digital calculation of the scalar diffraction," *J. Opt. Soc. Am. A* 29(9), 1956-1964 (2012).
- [14] L. Onural, "Some mathematical properties of the uniformly sampled quadratic phase function and associated issues in Fresnel diffraction simulations," *Opt. Eng.* 43(11), 2557-2563 (2004).
- [15] B. B. Mandelbrot, *The Fractal Geometry of Nature* (Freeman, 1982).
- [16] T.-C. Poon and J.-P. Liu, *Introduction to Modern Digital Holography with MATLAB* (Cambridge, 2014).
- [17] E. Carcole, J. Campos, I. Juvells, and S. Bosch, "Diffraction theory of low-resolution Fresnel encoded lenses," *Appl. Opt.* 33(29), 6741-6746 (1994).
- [18] D. M. Cottrell, J. A. Davis, T. Hedman, and R. A. Lilly, "Multiple imaging phase-encoded optical elements written as programmable spatial light modulators," *Appl. Opt.* 29(17), 2505-

- 2509 (1990).
- [19] R. Shanker, Principles of Quantum Mechanics (Springer, 2008).
 - [20] J. R. Fienup, "Phase retrieval algorithms: a comparison," Appl. Opt. 21(15), 2758-2769 (1982).
 - [21] A. W. Lohmann and D. P. Paris, "Binary Fraunhofer holograms, generated by computer," Appl. Opt. 6(10), 1739-1748 (1967).
 - [22] T. Shimobaba and T. Ito, "Random phase-free computer-generated hologram," Opt. Express 23(7), 9549-9554 (2015).
 - [23] P.W.M. Tsang and T.-C. Poon, "Novel method for converting digital Fresnel hologram to phase-only hologram based on bidirectional error diffusion," Opt. Express 21(20), 23680-23686 (2013).
 - [24] B. G. Chae, "Wide viewing-angle holographic display apparatus and method for displaying holographic image," KR patent application 10-2020-0140439 (2020).

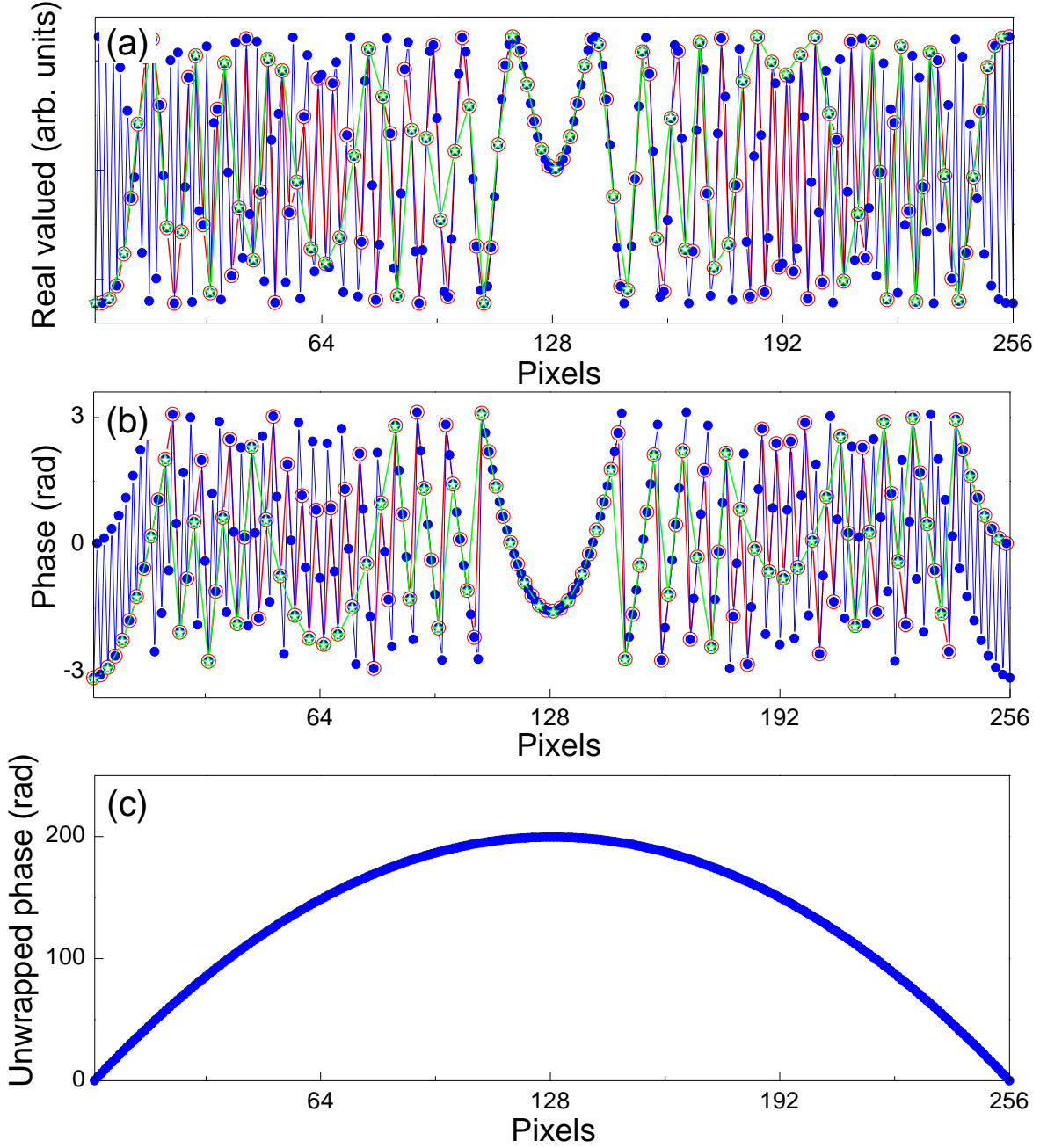


FIG. 1: Quadratic phase curves of (a) real-valued and (b) angle-valued PSFs are drawn in one-dimensional digitized space. The specifications of the blue curve are as follows; wavelength $\lambda = 532$ nm, distance $z = 30.8$ mm, pixel number $N = 256$, and pixel pitch $\Delta x = 8 \mu\text{m}$. The red and green curves are sampled by pixels of $2\Delta x$ and $4\Delta x$, respectively. (c) Unwrapped phase curve shows a smooth curvature.

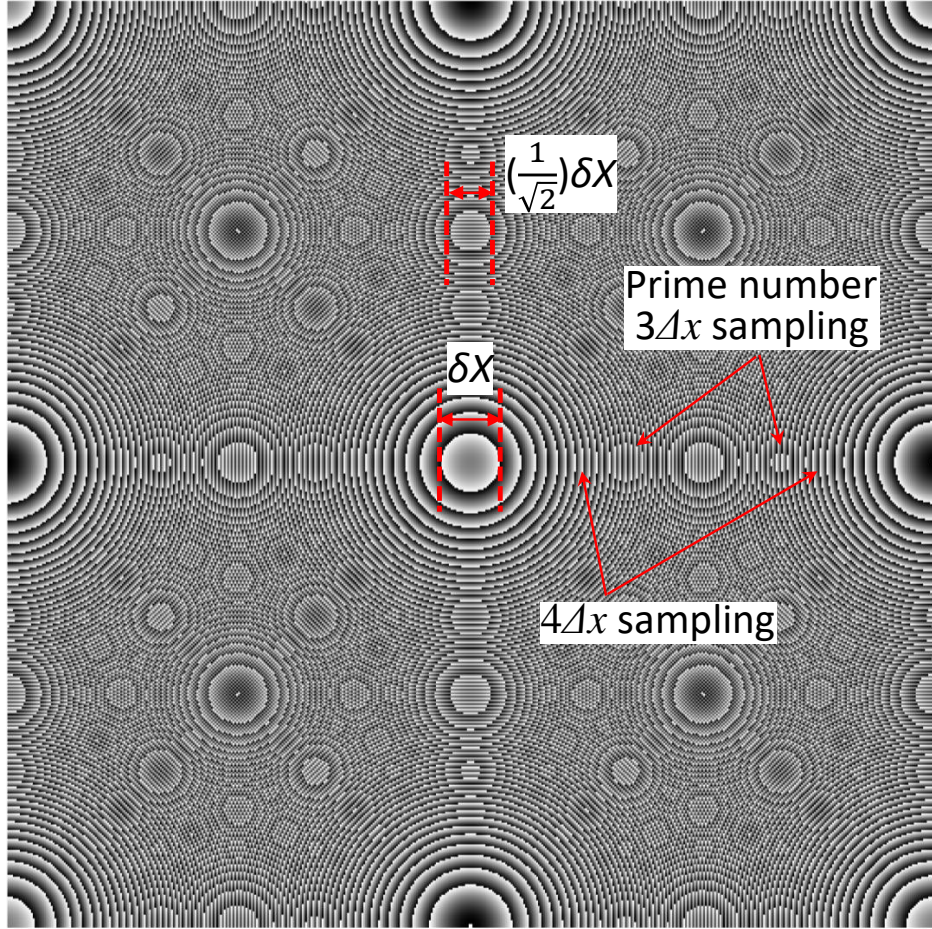


FIG. 2: Fractal structure of the sampled two-dimensional PSF. Angle-valued two-dimensional PSF, known as Fresnel zone plate, are drawn at specifications; distance of 7.7 mm and 512×512 pixels with a pixel pitch of $4 \mu\text{m}$. The four aliased fringes are generated in this specification, and δX indicates the width of core shell of the primary Fresnelet.

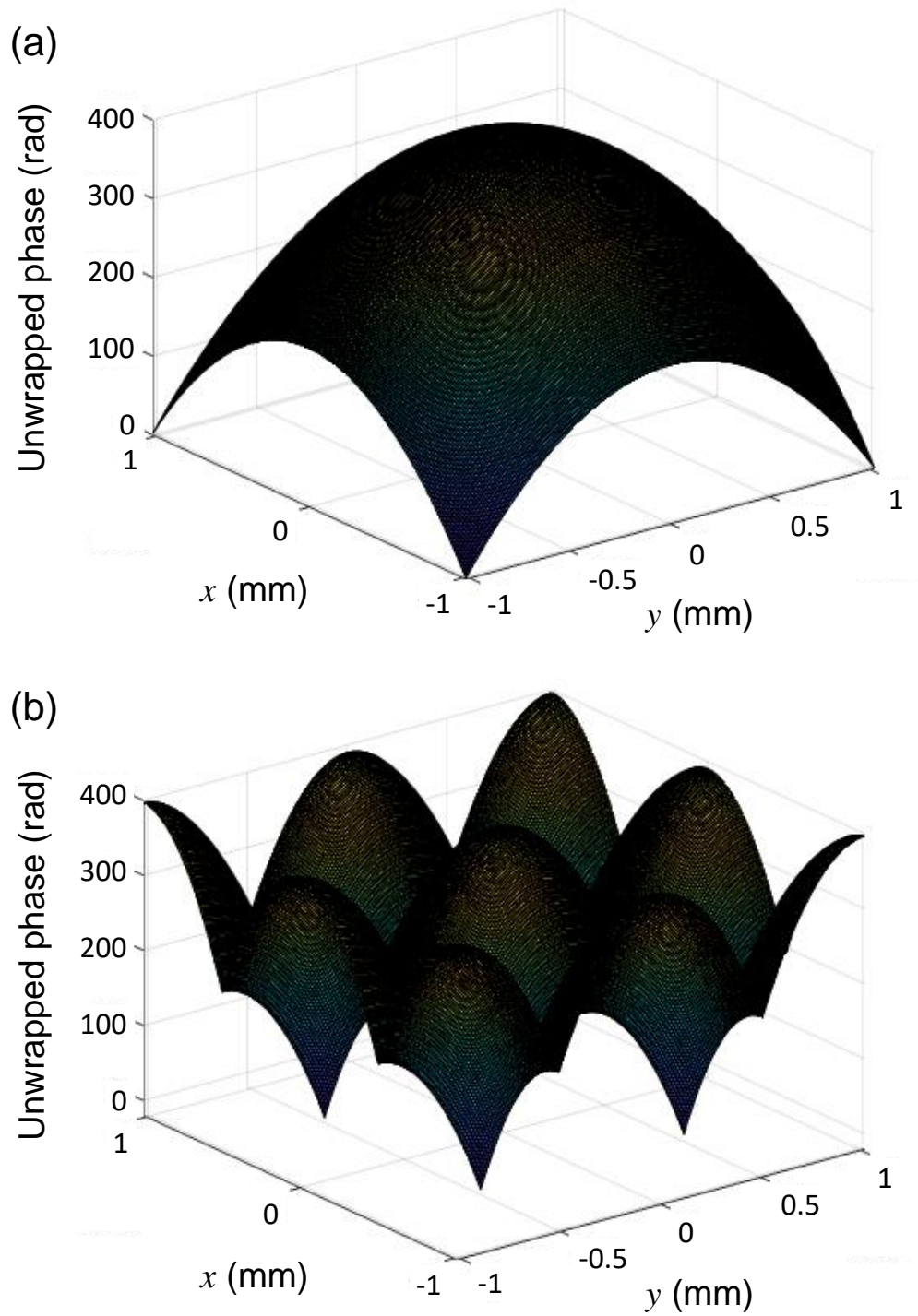


FIG. 3: Unwrapped phase of Fresnel zones synthesized at (a) a critical distance z_c and (b) a half of distance z_c . The specifications are as follows; wavelength $\lambda = 532$ nm, distance $z_c = 30.8$ mm, pixel number $N = 256$, and pixel pitch $\Delta x = 8 \mu\text{m}$.

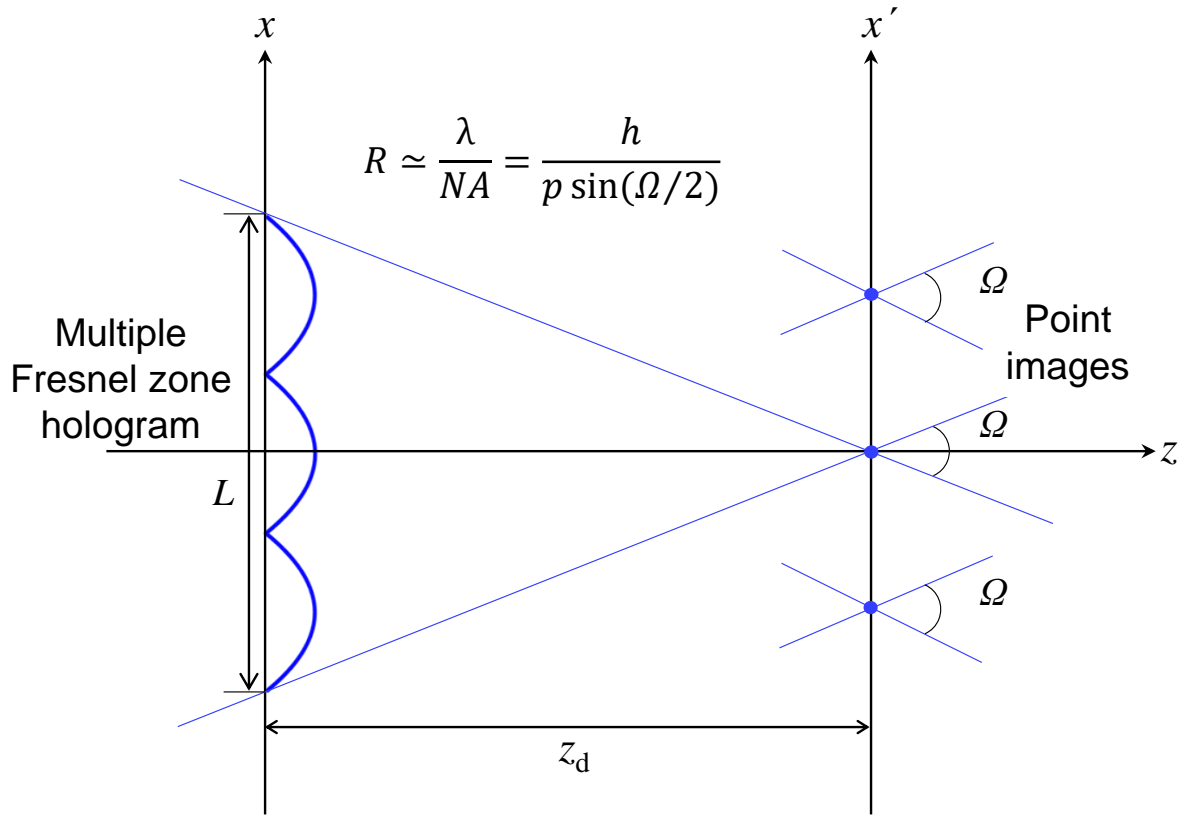


FIG. 4: Schematic diagram for analyzing the viewing angle of reconstructed point images from the enhanced-NA hologram. The multiple images have the same viewing angle within the quantum mechanical uncertainty relation.

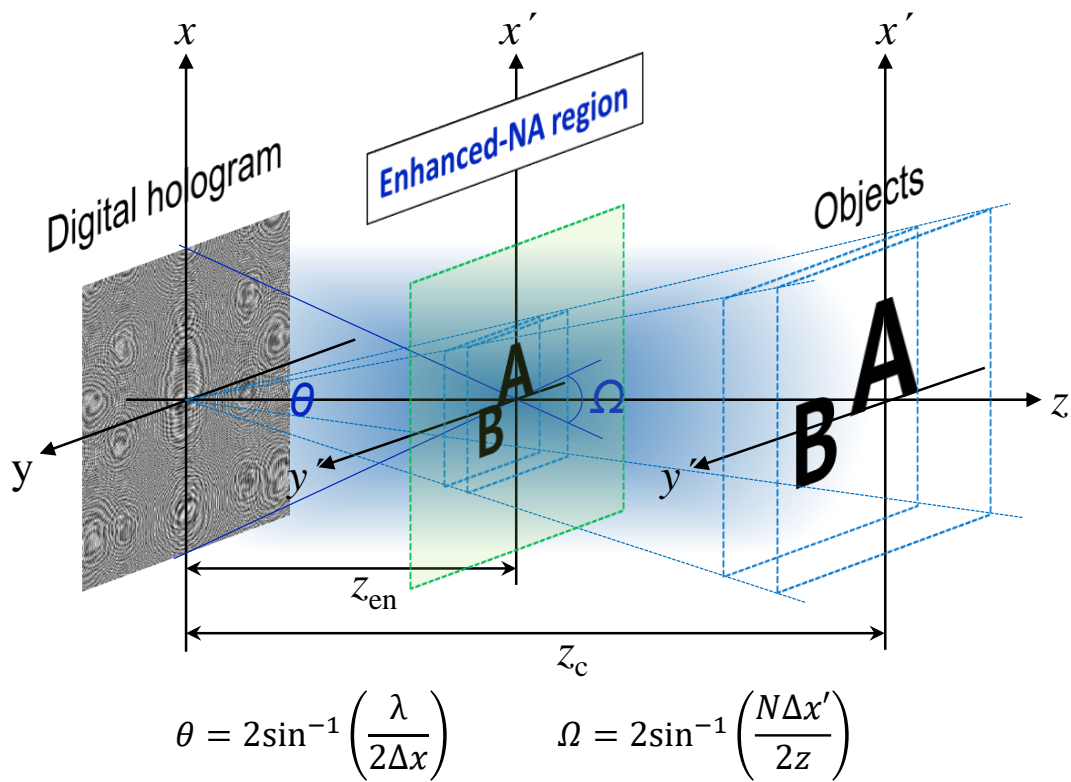


FIG. 5: Schematic of enhanced-NA hologram synthesis via the in-line holographic system. The physical sizes of the hologram and object are the same at a distance z_c . The amplitude hologram synthesized by Gerchberg-Saxton iterative algorithm is displayed. θ is the diffraction angle from pixel pitch Δx of hologram.

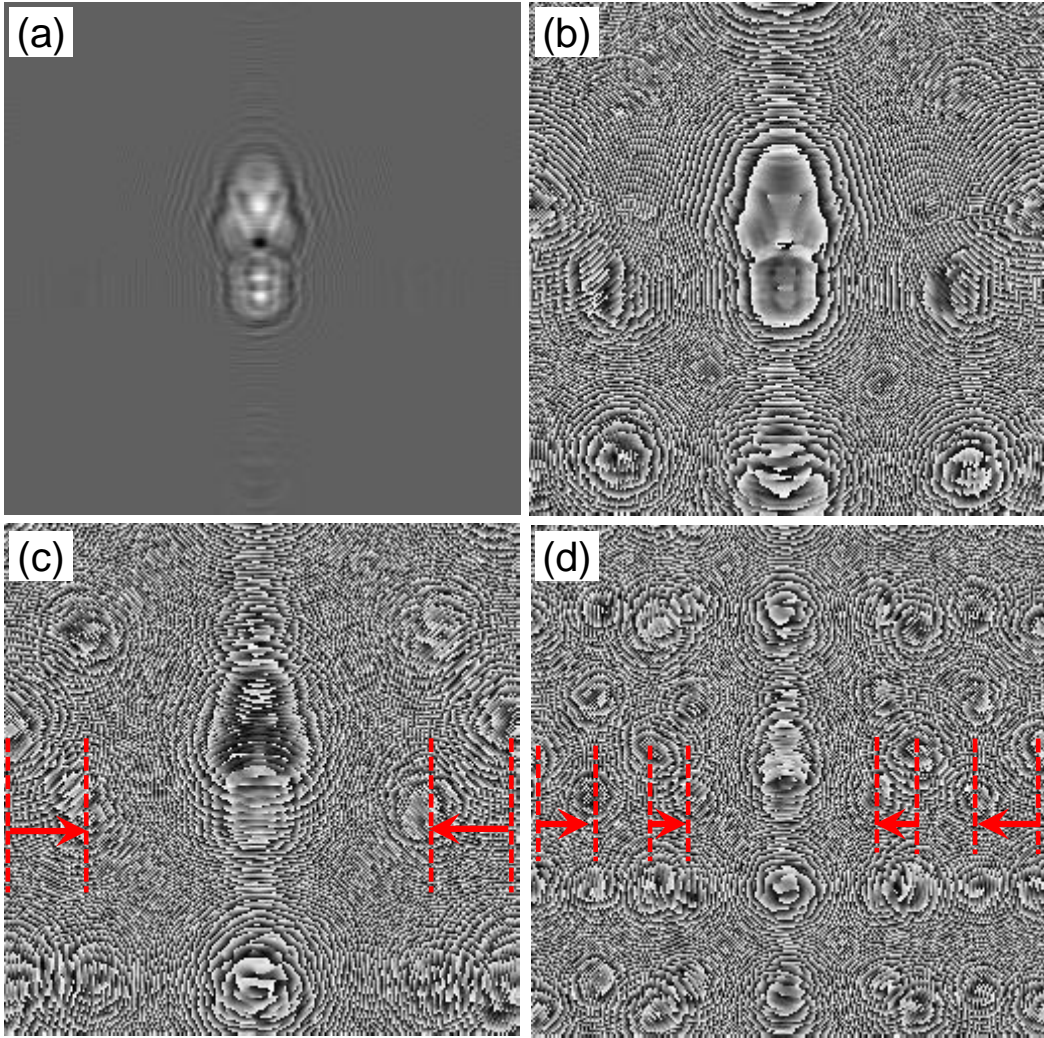


FIG. 6: Enhanced-NA hologram synthesized through the in-line holographic system. A digital hologram with 256×256 pixels and a pixel pitch of $8 \mu\text{m}$ is displayed to discriminate apparently the high-order fringes. (a) Real-valued and (b) angle-valued digital holograms of two letter objects synthesized at half the distance of z_c . The two letters are separated by 5 mm. (c) Phase hologram synthesized by the Gerchberg-Saxton iterative algorithm with 30 steps. The red arrow indicates the shift of the first letter fringes. (d) Phase hologram of two letter objects synthesized at quarter the distance of z_c . The two letters are separated by 2 mm.

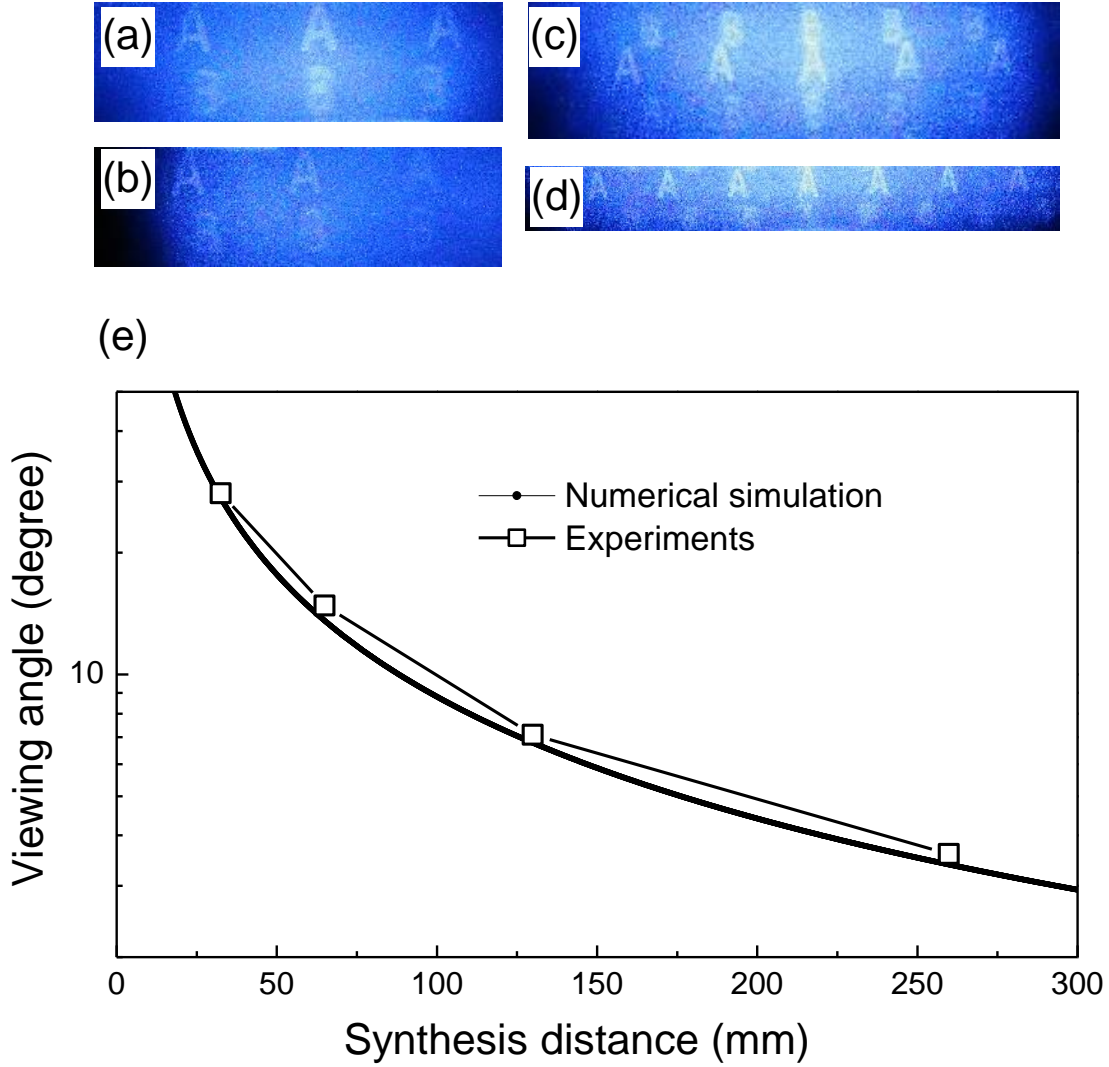


FIG. 7: Optically reconstructed images and their viewing angle variation from the enhanced-NA hologram. The images are captured at a slightly inclined vertical-direction to avoid the directed beam. (a) Reconstructed image of the digital hologram made at a distance of 129.9 mm. (b) Reconstructed image captured in the viewing direction of the first-order image. (c) Reconstructed image for the digital hologram made at a distance of 64.9 mm. (d) Reconstructed image for the digital hologram made at a distance of 32.5 mm. (e) Viewing angle variations of the holographic image as a function of the synthesis distance.